Linear-optical hyperentanglement-assisted quantum error-correcting code

Mark M. Wilde
Center for Quantum Information Science and Technology, Department of Electrical Engineering, University of Southern California, Los Angeles, California 90089, USA

Dmitry B. Uskov
Department of Physics, Tulane University, New Orleans, Louisiana 70118, USA
and Hearne Institute for Theoretical Physics, Department of Physics and Astronomy, Louisiana State University, Baton Rouge, Louisiana 70803, USA

(Received 22 August 2008; published 5 February 2009)

We propose a linear-optical implementation of a hyperentanglement-assisted quantum error-correcting code. The code is hyperentanglement assisted because the shared entanglement resource is a photonic state hyperentangled in polarization and orbital angular momentum. It is possible to encode, decode, and diagnose channel errors using linear-optical techniques. The code corrects for polarization "flip" errors and is thus suitable only for a proof-of-principle experiment. The encoding and decoding circuits use a Knill-Laflamme-Milburn-like scheme for transforming polarization and orbital angular momentum photonic qubits. A numerical optimization algorithm finds a unit-fidelity encoding circuit that requires only three ancilla modes and has success probability equal to 0.0097.

DOI: 10.1103/PhysRevA.79.022305 PACS number(s): 03.67.Pp, 03.67.Hk, 03.67.Lx, 42.50.Ex

I. INTRODUCTION

Quantum error correction plays an active role in the future realization of a quantum communication system [1,2]. Several optical experiments have already implemented simple quantum error-correction routines [3–5].

The entanglement-assisted stabilizer formalism is a recent extension of the theory of quantum error correction that incorporates entanglement shared between a sender and receiver [6,7]. A further extension of this theory incorporates gauge qubits [8] and others give a structure appropriate for a stream of quantum information [9–11]. The likely candidate for implementing an entanglement-assisted code is photonics because the entanglement-assisted model is more appropriate for quantum communication rather than quantum computing.

In this paper, we propose a linear-optical implementation of a hyperentanglement-assisted quantum code. Our code is hyperentanglement assisted because it exploits hyperentanglement of two photons [12]. Two photons are hyperentangled if they have entanglement in multiple degrees of freedom such as polarization and orbital angular momentum (OAM) [13,14]. The benefit of hyperentanglement is that a linear-optical setup suffices to perform a complete Bell-state analysis [15–17]. Our proposal for the hyperentanglement-assisted code relies on the recent optical realization [18] of the superdense coding protocol [19] and the close connection between entanglement-assisted quantum error correction and superdense coding [7]. We also employ a recent numerical optimization algorithm [20] to find an encoding circuit and a decoding circuit that has unit fidelity, success probability equal to 0.0097, and requires only three ancilla modes. The circuits act on both the polarization and OAM degrees of freedom of the photonic qubits.

We structure this paper as follows. The first section reviews hyperentangled states, the single-photon polarization-OAM states, and mentions that it is possible to distinguish the single-photon polarization-OAM states with linear optics. We then discuss the superdense coding protocol for hyperentangled states and highlight the connection between superdense coding and entanglement-assisted quantum error correction. We give a brief description of our code, its error analysis, and corrective operations. The final part of this paper discusses the numerical optimization technique for finding our code's encoding circuit and decoding circuit.

II. HYPERENTANGLED STATES

The standard hyperentangled state is a state of two photons simultaneously entangled in polarization and OAM:

$$\tfrac{1}{2}(|HH\rangle + |VV\rangle) \otimes (|\circlearrowleft\ \circlearrowleft\rangle + |\circlearrowright\ \circlearrowright\rangle).$$

The symbols H and V represent horizontal and vertical polarization, respectively, and the symbols $\circlearrowleft$ and $\circlearrowright$ represent paraxial Laguerre-Gauss spatial modes with $+\hbar$ and $-\hbar$, respective units of OAM [21]. Changing the polarization degree of freedom of Alice's photon in the above state according to the four standard Pauli operators, while leaving the OAM degree of freedom unchanged, gives the following four hyperentangled states:

$$|\Phi^{\pm}\rangle \equiv \tfrac{1}{2}(|HH\rangle \pm |VV\rangle) \otimes (|\circlearrowleft\ \circlearrowleft\rangle + |\circlearrowright\ \circlearrowright\rangle),$$

$$|\Psi^{\pm}\rangle \equiv \tfrac{1}{2}(|HV\rangle \pm |VH\rangle) \otimes (|\circlearrowleft\ \circlearrowright\rangle + |\circlearrowright\ \circlearrowleft\rangle). \quad (1)$$

We can rewrite the above four states in terms of the single-photon polarization-OAM states $\phi^{\pm}, \psi^{\pm}$ [30],

$$|\Phi^{\pm}\rangle = \tfrac{1}{4}(\phi_A^{+} \otimes \psi_B^{\pm} + \phi_A^{-} \otimes \psi_B^{\mp} + \psi_A^{+} \otimes \phi_B^{\pm} + \psi_A^{-} \otimes \phi_B^{\mp}),$$

$$|\Psi^{\pm}\rangle = \tfrac{1}{4}(\pm\phi_A^{+} \otimes \phi_B^{\pm} \mp \phi_A^{-} \otimes \phi_B^{\mp} \pm \psi_A^{+} \otimes \psi_B^{\pm} \mp \psi_A^{-} \otimes \psi_B^{\mp}),$$

where A and B label the first and second respective photons and the single-photon polarization-OAM states $\phi^{\pm}$ and $\psi^{\pm}$ are as follows:

$$\phi^{\pm} \equiv \frac{|H\circlearrowleft\rangle \pm |V\circlearrowright\rangle}{\sqrt{2}}, \quad \psi^{\pm} \equiv \frac{|H\circlearrowright\rangle \pm |V\circlearrowleft\rangle}{\sqrt{2}}.$$

The above "quad-rail" basis states $|H\circlearrowleft\rangle$, $|H\circlearrowright\rangle$, $|V\circlearrowleft\rangle$, $|V\circlearrowright\rangle$ are four-mode single-photon states defined in terms of the Fock basis,

$$|H\circlearrowleft\rangle \equiv |1\rangle_{H\circlearrowleft}|0\rangle_{H\circlearrowright}|0\rangle_{V\circlearrowleft}|0\rangle_{V\circlearrowright},$$

$$|H\circlearrowright\rangle \equiv |0\rangle_{H\circlearrowleft}|1\rangle_{H\circlearrowright}|0\rangle_{V\circlearrowleft}|0\rangle_{V\circlearrowright},$$

$$|V\circlearrowleft\rangle \equiv |0\rangle_{H\circlearrowleft}|0\rangle_{H\circlearrowright}|1\rangle_{V\circlearrowleft}|0\rangle_{V\circlearrowright},$$

$$|V\circlearrowright\rangle \equiv |0\rangle_{H\circlearrowleft}|0\rangle_{H\circlearrowright}|0\rangle_{V\circlearrowleft}|1\rangle_{V\circlearrowright}. \quad (2)$$

Hyperentangled states are useful because a linear-optical analyzer distinguishes the single-photon polarization-OAM states $\phi^{\pm}, \psi^{\pm}$ and thus distinguishes the hyperentangled states $|\Phi^{\pm}\rangle$, $|\Psi^{\pm}\rangle$ as well [15–17].

III. SUPERDENSE CODING AND ENTANGLEMENT-ASSISTED QUANTUM ERROR CORRECTION

We briefly describe the superdense coding protocol for polarization encoding and hyperentangled states [18]. A sender Alice and a receiver Bob share a hyperentangled state $|\Phi^{+}\rangle^{AB}$. Alice encodes one of four classical messages (two classical bits) by applying one of four transformations to her half of $|\Phi^{+}\rangle^{AB}$: (1) The identity, (2) $|V\rangle \rightarrow -|V\rangle$, (3) $|H\rangle \leftrightarrow |V\rangle$, or (4) both $|V\rangle \rightarrow -|V\rangle$ and $|H\rangle \leftrightarrow |V\rangle$. Let Z denote the second operation and let X denote the third operation. The result is to transform the original state $|\Phi^{+}\rangle^{AB}$ to one of the four states $|\Phi^{\pm}\rangle^{AB}, |\Psi^{\pm}\rangle^{AB}$. She then sends her half of the encoded $|\Phi^{+}\rangle^{AB}$ to Bob. Bob performs a single-photon polarization-OAM state analysis in the basis $\phi^{\pm}, \psi^{\pm}$ on each of the systems A and B to distinguish the message Alice transmitted.

In the above analysis, it is important to stress that the dense coding transformations affect only the polarization degree of freedom of the hyperentangled state $|\Phi^{+}\rangle^{AB}$. The classical information resides in a four-dimensional subspace of the 16-dimensional Hilbert space. The extra dimensions help in single-photon polarization-OAM state analysis in order to distinguish the classical messages.

Reference [7] discusses the close relationship between superdense coding and entanglement-assisted quantum error correction. In superdense coding, one exploits the classical bits encoded in a Bell state so that Alice can transmit classical information to Bob. In entanglement-assisted error correction, one exploits the encoded classical bits for use as error syndromes. Another way of thinking about this latter scenario is that Eve, the environment, is superdense coding messages (errors) into the Bell states. Bob can determine the errors that Eve introduces by measuring in the Bell basis.

IV. OPERATION OF THE CODE

The operation of our code begins with an initial, unencoded state consisting of one information photon and one hyperentangled state,

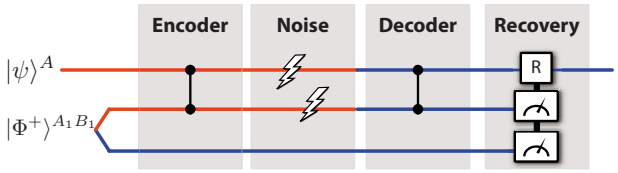

FIG. 1. (Color online) The operation of the hyperentanglement-assisted quantum code. The qubits labeled as A and A_1 (red in the online version) belong to the sender Alice and the qubit labeled as B_1 (blue in the online version) belongs to the receiver Bob though all qubits belong to Bob after the noisy channel. Alice and Bob share a hyperentangled state $|\Phi^{+}\rangle^{A_1B_1}$ prior to quantum communication. Alice uses the hyperentangled state to aid in encoding an information photon in the state $|\psi\rangle^{A}$. Her encoding circuit consists of one controlled-phase gate. She sends her photons over a noisy polarization-error quantum channel. Bob receives the photons, performs a decoding circuit, and performs two single-photon polarization-OAM analyses in the basis $\phi^{\pm}, \psi^{\pm}$ on the systems A_1 and B_1 to determine the error syndrome. Bob finally performs a recovery operation to obtain the information photon $|\psi\rangle^{A}$ that Alice first sent.

$$|\psi\rangle^{A}|\Phi^{+}\rangle^{A_1B_1}. \quad (3)$$

The information photon is as follows: $|\psi\rangle^{A} \equiv \alpha|H\rangle^{A} + \beta|V\rangle^{A}$. The sender Alice possesses photons A and A_1 and the receiver Bob possesses photon B_1. The entanglement-assisted communication paradigm assumes that Alice and Bob share the hyperentangled state prior to quantum communication. Figure 1 highlights the operation of our hyperentanglement-assisted quantum code.

The sender Alice applies an encoding circuit consisting of one controlled-sign gate (we discuss this gate later in more detail) so that the state shared between Alice and Bob is the following unnormalized encoded state:

$$|\psi\rangle^{A}(|\Phi^{-}\rangle^{A_1B_1} + |\Phi^{+}\rangle^{A_1B_1}) + Z|\psi\rangle^{A}(|\Phi^{+}\rangle^{A_1B_1} - |\Phi^{-}\rangle^{A_1B_1}). \quad (4)$$

She sends her photons A and A_1 over a noisy polarization-error channel (discussed below). Bob receives the photons and we relabel them as B and B_1', respectively. For now, suppose that the channel does not introduce an error. Bob finally applies the decoding circuit (same as the encoding circuit) and the resulting decoded state is as follows:

$$|\psi\rangle^{B}|\Phi^{+}\rangle^{B_1'B_1}, \quad (5)$$

where the information photon appears in Bob's system B. Bob performs two single-photon polarization-OAM analyses in the basis $\phi^{\pm}, \psi^{\pm}$ on the systems B_1' and B_1 to diagnose the channel error. The polarization-OAM analysis distinguishes the four states $\{|\Phi^{\pm}\rangle, |\Psi^{\pm}\rangle\}$. Bob measures the result $|\Phi^{+}\rangle$ when the channel does not introduce noise. The state $|\Phi^{+}\rangle$ is a syndrome that determines the channel error. Bob does not need to perform a recovery operation in this case.

V. ERROR ANALYSIS

In general, the channel introduces errors on the photons that Alice transmits. We assume in this paper that the channel

TABLE I. The table details the results of Bob's Bell state analysis. The states in the third column are syndromes that determine the channel error ("error") and the recovery operation ("recovery") that Bob should perform to recover the initial information photon.

Error	Recovery	Syndrome
I	I	Φ^+
X^A	X	Φ^-
X^{A_1}	Z	Ψ^+
$X^A X^{A_1}$	ZX	Ψ^-

is a noisy polarization-error channel (analogous to the classical bit-flip channel). A noisy polarization-error channel independently applies a polarization error X that flips the horizontal and vertical polarization bases. We assume that this channel affects the polarization degree of freedom only and does not affect the OAM degree of freedom. Although this channel may not be entirely realistic, it provides a platform for a proof-of-principle demonstration of the operation of an entanglement-assisted quantum code [31].

The code protects against a single polarization error on either of the two photons A or A_1 that Alice sends. It also protects against a double polarization error on both photons. Suppose that a polarization error occurs on photon A. After Bob applies the decoding circuit, the state becomes $X|\psi\rangle^B|\Phi^-\rangle^{B_1' B_1}$. Bob measures the photons B_1' and B_1, determines they are in the state $|\Phi^-\rangle$, and flips the polarization of photon B to recover the initial information photon $|\psi\rangle$. Table I summarizes the other cases.

VI. OPTICAL ENCODING AND DECODING CIRCUIT

The seminal paper of Knill, Laflamme, and Milburn (KLM) showed how to perform two-qubit interactions with linear-optical devices [22,23]. Their method is a measurement-assisted scheme. It first mixes a set of "computational " modes and ancilla modes in a linear-optical device and then counts the photons in the ancilla modes. The optical transformation acts on the computational modes. The ancilla modes help perform this transformation and we measure them at the end of the measurement-assisted scheme. The gates exploit the Hong-Ou-Mandel quantum interference of indistinguishable photons [24]. These measurement-assisted transformations are heralded, nondeterministic, and nondestructive. A destructive gate involves a measurement on the computational modes—the informational state collapses to one of the states in the measurement basis even when the gate succeeds. A nondestructive gate requires a measurement only on the ancilla modes—the result is that all the information encoded in the state remains intact when the gate succeeds [23,25].

The measurement-assisted scheme is useful for dual-rail encoded qubits and even polarization-encoded qubits [26], but until now, no one has considered its application to "quad-rail " encoded quantum information in polarization-OAM states.

The implementation of a polarization-OAM measurement-assisted scheme requires unconventional linear-optical elements analogous to beam splitters and other tools of linear optics acting on OAM states of photons. Holographic elements suffice for this purpose because they act on OAM components [18]—similarly to the action of polarization beam splitters on photon polarization. The extension of the measurement-assisted scheme to OAM states is a generalization of the idea in Ref. [26]. There, the authors extended the measurement-assisted scheme to polarization-encoded qubits. Here, we use a similar idea to extend the measurement-assisted scheme to OAM states.

The encoding transformation corresponding to our code generates the encoded state in (4). It is a controlled-sign gate that acts on the four-dimensional Hilbert space $\mathcal{H}_A \otimes \mathcal{H}_{A_1}$ of the information photon A and the polarization subspace of Alice's part A_1 of the hyperentangled state in (3). The gate acts on the polarization degrees of freedom and leaves the OAM degrees of freedom invariant. It is a linear-optical transformation on a set of six modes—two modes for the A system and four modes for the A_1 system. The gate leaves the following basis states:

$$|H\rangle^A|H\circlearrowleft\rangle^{A_1},\quad |H\rangle^A|H\circlearrowright\rangle^{A_1},\quad |H\rangle^A|V\circlearrowleft\rangle^{A_1},$$

$$|H\rangle^A|V\circlearrowright\rangle^{A_1},\quad |V\rangle^A|H\circlearrowleft\rangle^{A_1},\quad |V\rangle^A|H\circlearrowright\rangle^{A_1}, \tag{6}$$

invariant and adds a phase to the remaining basis states,

$$|V\rangle^A|V\circlearrowleft\rangle^{A_1} \rightarrow -|V\rangle^A|V\circlearrowleft\rangle^{A_1},$$

$$|V\rangle^A|V\circlearrowright\rangle^{A_1} \rightarrow -|V\rangle^A|V\circlearrowright\rangle^{A_1}. \tag{7}$$

We make a statement about the mathematical structure of the Hilbert space of polarization-OAM states. It is possible to decompose any Hilbert space with a tensor product structure. For example,

$$\text{span}\{|H\circlearrowleft\rangle,|V\circlearrowleft\rangle,|H\circlearrowright\rangle,|V\circlearrowright\rangle\}$$
$$= \text{span}\{|H\rangle,|V\rangle\} \otimes \text{span}\{|\circlearrowleft\rangle,|\circlearrowright\rangle\}.$$

While in the paraxial approximation, local optical transformations on the subspaces span $\{|H\rangle,|V\rangle\}$ and span $\{|\circlearrowleft\rangle, |\circlearrowright\rangle\}$ respect the tensor-product decomposition of the full four-dimensional space. However, the tensor-product notation in Eq. (1) from Ref. [18] may be somewhat misleading in the context of a measurement-assisted transformation (which the authors of Ref. [18] do not discuss). A qubit-coupling measurement-assisted transformation, based on the mixing of creation operators in separate modes, does not respect such a tensor-product decomposition in general. Instead such an operation acts naturally on a space constructed as a direct sum, e.g., span $\{|H\circlearrowleft\rangle,|V\circlearrowleft\rangle\}\oplus$ span $\{|H\circlearrowright\rangle,|V\circlearrowright\rangle\}$. The above restriction places a constraint on the form of the linear-optical encoding circuit and decoding circuit.

Knill devised an optimal solution for the controlled-sign gate [27]. We could use Knill's two dual-rail qubit gate for an implementation of the transformation in (7). It requires the combination of two separate transforms: The first acts on the $\circlearrowleft$ OAM states and the second acts on the $\circlearrowright$ OAM states. Each transformation requires two ancilla modes and has a

success probability of 2/27 [27]. This "Knill combination" scheme thus requires four ancilla modes with a success probability of $(2/27)^2 \approx 0.0055$.

We have employed the numerical optimization technique in Ref. [20] for our encoding circuit rather than the above Knill combination scheme. Our optical scheme for the encoding transformation in (6) and (7) requires only three ancilla photons and has a success probability of 0.0097 (nearly a twofold increase over the Knill combination scheme).

We briefly describe the numerical optimization technique for finding a general linear-optical circuit [20]. An $N \times N$ matrix, where N is the number of optical modes, completely characterizes an optical transformation. The numerical implementation of the optimization algorithm performs a gradient search in the space of these matrices. The algorithm first finds a matrix that guarantees a unit transformation fidelity and then performs a constrained optimization of success probability in the unit fidelity subspace. Each optimization cycle ends at some local maximum of success probabilitiy. The resulting Kraus transformation, or contraction map, acting on the computational modes matches the desired target transformation in the case of a successful measurement outcome on the ancilla modes.

We now describe the results of the procedure for our case where the encoding circuit acts on the modes for Alice's systems A and A_1 and three ancilla modes. We performed the optimization in the 81-dimensional complex space of a GL(9) matrix (six modes for Alice's systems A and A_1 and three ancilla modes). Such a matrix admits a decomposition into a sequence of operations where each operation corresponds to a standard optical element [28]. We were able to simplify the transformation even more by using a technique from Ref. [27]. The optimal transformation actually acts on three modes only: The vertical polarization of Alice's photon A, the vertical polarization and $\circlearrowleft$ OAM of Alice's photon A_1, and the vertical polarization and $\circlearrowright$ OAM of Alice's photon A_1. The reduction of the optimal solution to a three-mode operation should make it easier to implement experimentally. The following equations illustrate the reduced transformation:

$$|n_1\rangle_V^A |n_2\rangle_{V\circlearrowleft}^{A_1} \rightarrow (-1)^{f(n_1,n_2)} |n_1\rangle_V^A |n_2\rangle_{V\circlearrowleft}^{A_1},$$

$$|n_1\rangle_V^A |n_2\rangle_{V\circlearrowright}^{A_1} \rightarrow (-1)^{f(n_1,n_2)} |n_1\rangle_V^A |n_2\rangle_{V\circlearrowright}^{A_1},$$

where n_1 and n_2 are photon numbers equal to either zero or one and the function f is equal to one if $n_1 = n_2 = 1$ and is equal to zero otherwise. One can verify that the implementation of the above reduced transformation is equivalent to the full transformation in (7). Figure 2 illustrates a sample distribution of success probabilities in increasing order.

The best found solution provides a success probability of 0.009 742 76 at a fidelity of $1-(6\times10^{-8})$. This solution, most likely, is the optimal global solution, or at least close to the global optimum. One cannot verify the global character of a solution by numerical tools only. However, we have found that further optimization with the current scheme does not improve the result. The success probability shows a slight increase for nonunit fidelity: At the level of 0.99 fidelity, we have found a solution with success probability of 0.011. Further relaxing the unit fidelity requirement does not lead to any significant increase of the success probability.

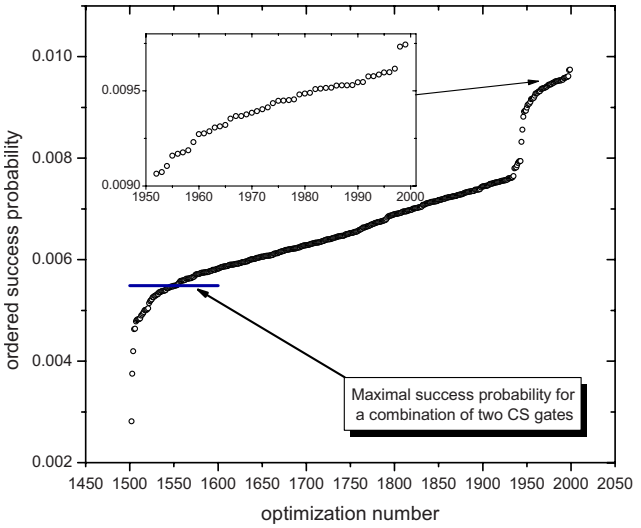

FIG. 2. (Color online) The figure displays the results of the numerical gate optimization algorithm for our case of six computational modes and three ancilla modes. The algorithm starts an optimization at a randomly selected point in the space of 6×6 matrices and maximizes the gate fidelity. The second stage of the optimization algorithm is a constrained optimization of success probability within the unit fidelity subspace. The figure displays ordered success probability for the best 500 optimization cycles of the total amount of 2000 optimizations for fidelity $>1-10^{-7}$. The algorithm finds an encoding circuit with a success probability almost 2 times that of the Knill combination scheme.

We now address the issue of implementing our hyperentanglement-assisted quantum code. As described above, our encoding circuit solution corresponds to some optical transformation matrix. The first question arising in connection with the possible experimental implementation of such an optical transformation is whether the obtained matrix is unitary. Currently, we use an optimization algorithm that searches for an arbitrary matrix, one not necessarily restricted to the subspace of unitary matrices. Therefore, one may need to apply a unitary dilation procedure [27,29] to embed the matrix into a larger unitary matrix. However, a solution corresponding to a maximal success probability is a matrix requiring minimal dilation, due to the singular behavior of the gradient of the success probability function on the manifold of unitary matrices. Indeed the two best solutions (see inset in Fig. 2) correspond to matrices with the following singular values {1, 1, 1, 1, 1, 0.5}. One needs to introduce only one additional vacuum mode to embed the matrix into an SU(7) matrix in order to implement the transformation in the form of beam splitters and phase shifters. Reference [28] suggests the scheme of such a decomposition. Mathematically, it corresponds to a factorization of an arbitrary SU(N) matrix into a product of SU(2) matrices. The implementation in Ref. [28] requires $N(N-1)/2$ beam splitters. However, it is well known that in some important cases one can find a simpler decomposition [27]. Knill's scheme requires only four beam splitters for the realization of an SU(4) matrix, whereas the original KLM scheme requires eight beam split-

ters for an SU(6) matrix. The matrix we have obtained is rather complicated because we were not able to find a "nice" decomposition (see the Appendix for the matrix).

VII. CONCLUSION

We have presented an optical implementation of an entanglement-assisted quantum code that should be realizable with current technology. The code encodes one information photon with the help of a hyperentangled state.

ACKNOWLEDGMENTS

The authors thank Todd A. Brun for useful discussions. M.M.W. acknowledges support from NSF Grant No. 0545845 and D.B.U. acknowledges support from the Army Research Office and the Intelligence Advanced Research Projects Activity.

APPENDIX

Below we list the matrix that implements the transformation for the encoding circuit. We do not provide it as one large matrix because the individual entries are too large, but instead provide it a few columns at a time. The first three columns are as follows:

$$\begin{bmatrix} -0.253\,936 + i0.215\,424 & 0 & -0.0269\,989 + i0.211\,134 \\ 0 & 1 & 0 \\ 0.0473\,299 + i0.183\,042 & 0 & -0.136\,174 + i0.454\,254 \\ 0 & 0 & 0 \\ 0.196\,523 - i0.216\,478 & 0 & -0.233\,841 + i0.184\,769 \\ 0 & 0 & 0 \\ -0.33\,549 - i0.135\,251 & 0 & 0.314\,695 + i0.192\,451 \\ 0.318\,659 + i0.380\,869 & 0 & 0.3053 + i0.314\,815 \\ 0.277\,613 - i0.411\,775 & 0 & -0.0145\,173 + i0.484\,746 \end{bmatrix}.$$

The second three columns are as follows:

$$\begin{bmatrix} 0 & -0.249\,991 - i0.213\,976 & 0 \\ 0 & 0 & 0 \\ 0 & 0.262\,553 + i0.141\,112 & 0 \\ \alpha & 0 & 0 \\ 0 & -0.159\,651 + i0.187\,183 & 0 \\ 0 & 0 & \alpha \\ 0 & -0.515\,822 + i0.243\,508 & 0 \\ 0 & 0.220\,057 - i0.296\,955 & 0 \\ 0 & 0.039\,117 + i0.303\,606 & 0 \end{bmatrix},$$

where $\alpha = -0.611\,421 - i0.791\,452$. The next two columns are as follows:

$$\begin{bmatrix} 0.410\,744 + i0.0245\,062 & 0.367\,852 - i0.184\,455 \\ 0 & 0 \\ -0.4806 - i0.326\,223 & 0.298\,488 - i0.221\,226 \\ 0 & 0 \\ -0.264\,695 - i0.0518\,749 & 0.153\,492 + i0.498\,569 \\ 0 & 0 \\ -0.238\,16 - i0.143\,929 & -0.278\,242 - i0.005\,318\,07 \\ 0.132\,686 - i0.193\,403 & -0.0860\,369 + i0.415\,03 \\ 0.382\,029 + i0.183\,596 & -0.229\,701 + i0.0475\,146 \end{bmatrix}.$$

The last column is as follows:

$$\begin{bmatrix} -0.0349\,526 + i0.229\,345 \\ 0 \\ -0.0337\,073 + i0.290\,301 \\ 0 \\ 0.403\,926 - i0.202\,786 \\ 0 \\ -0.337\,872 - i0.218\,04 \\ -0.334\,824 - i0.268\,026 \\ -0.164\,744 + i0.395\,987 \end{bmatrix}.$$

[1] A. R. Calderbank, E. M. Rains, P. W. Shor, and N. J. A. Sloane, IEEE Trans. Inf. Theory **44**, 1369 (1998).
[2] D. Gottesman, Ph. D. thesis, California Institute of Technology, 1997.
[3] J. L. O'Brien, G. J. Pryde, A. G. White, and T. C. Ralph, Phys. Rev. A **71**, 060303(R) (2005).
[4] T. B. Pittman, B. C. Jacobs, and J. D. Franson, Phys. Rev. A **71**, 052332 (2005).
[5] Z. Zhao, Y.-A. Chen, A.-N. Zhang, T. Yang, H. J. Briegel, and J.-W. Pan, Nature (London) **430**, 54 (2004).
[6] T. A. Brun, I. Devetak, and M.-H. Hsieh, Science **314**, 436 (2006).
[7] T. A. Brun, I. Devetak, and M.-H. Hsieh, e-print arXiv:quant-ph/0608027v2.
[8] M.-H. Hsieh, I. Devetak, and T. Brun, Phys. Rev. A **76**, 062313 (2007).
[9] M. M. Wilde, H. Krovi, and T. A. Brun, e-print arXiv:0708.3699.
[10] M. M. Wilde and T. A. Brun, e-print arXiv:0712.2223.
[11] M. M. Wilde and T. A. Brun, e-print arXiv:0807.3803.
[12] P. G. Kwiat, J. Mod. Opt. **44**, 2173 (1997).
[13] J. T. Barreiro, N. K. Langford, N. A. Peters, and P. G. Kwiat, Phys. Rev. Lett. **95**, 260501 (2005).
[14] G. Molina-Terriza, J. P. Torres, and L. Torner, Nat. Phys. **3**, 305 (2007).
[15] P. G. Kwiat and H. Weinfurter, Phys. Rev. A **58**, R2623 (1998).
[16] C. Schuck, G. Huber, C. Kurtsiefer, and H. Weinfurter, Phys. Rev. Lett. **96**, 190501 (2006).
[17] M. Barbieri, G. Vallone, P. Mataloni, and F. DeMartini, Phys.

Rev. A **75**, 042317 (2007).
[18] J. T. Barreiro, T.-C. Wei, and P. G. Kwiat, Nat. Phys. **4**, 282 (2008).
[19] C. H. Bennett and S. J. Wiesner, Phys. Rev. Lett. **69**, 2881 (1992).
[20] D. B. Uskov, L. Kaplan, A. M. Smith, S. D. Huver, and J. P. Dowling, e-print arXiv:0808.1926.
[21] *Optical Angular Momentum*, edited by L. Allen, S. M. Barnett, and M. J. Padgett (Institute of Physics, Bristol, 2003).
[22] E. Knill, R. Laflamme, and G. J. Milburn, Nature (London) **409**, 46 (2001).
[23] P. Kok, W. J. Munro, K. Nemoto, T. C. Ralph, J. Dowling, and G. Milburn, Rev. Mod. Phys. **79**, 135 (2007).
[24] C. K. Hong, Z. Y. Ou, and L. Mandel, Phys. Rev. Lett. **59**, 2044 (1987).
[25] X.-H. Bao, T.-Y. Chen, Q. Zhang, J. Yang, H. Zhang, T. Yang, and J.-W. Pan, Phys. Rev. Lett. **98**, 170502 (2007).
[26] F. M. Spedalieri, H. Lee, and J. P. Dowling, Phys. Rev. A **73**, 012334 (2006).
[27] E. Knill, Phys. Rev. A **66**, 052306 (2002).
[28] M. Reck, A. Zeilinger, H. J. Bernstein, and P. Bertani, Phys. Rev. Lett. **73**, 58 (1994).
[29] N. M. VanMeter, P. Lougovski, D. B. Uskov, K. Kieling, J. Eisert, and J. P. Dowling, Phys. Rev. A **76**, 063808 (2007).
[30] Reference [18] refers to these states as spin-orbit Bell states, but this name is inappropriate given that the states are encoded in polarization and orbital angular momentum and it is not clear whether these states could violate a Bell's inequality.
[31] We do have examples of hyperentanglement-assisted codes that can correct an arbitrary single-qubit error. But such codes either require more hyperentanglement or increase the complexity of our numerical optimization procedure (or do both). This increase in complexity conflicts with our main purpose in this paper—to suggest a minimal, proof-of-principle demonstration of entanglement-assisted error correction.